Mean Velocity and Moments of Turbulent Velocity Fluctuations in the Wake of a Model Ship Propulsor

João P. Pêgo[1], Hermann Lienhart[2], Franz Durst[2]

1: Faculty of Engineering, University of Porto, Porto, Portugal, jppego@fe.up.pt
2: LSTM-Erlangen, University of Erlangen-Nuremberg, Germany, lienhart@lstm.uni-erlangen.de, durst@lstm.uni-erlangen.de

Abstract Pod drives are modern outboard ship propulsion systems with a motor encapsulated in a watertight pod. The motor's shaft is connected directly to one or two propellers. The whole unit hangs from the stern of the ship and rotates azimuthally, thus providing thrust and steering without the need of a rudder.

Force/momentum and phase-resolved LDA measurements were performed for inline co-rotating and contra-rotating propellers pod drive models (see figure 1). The measurements permitted to characterize these ship propulsion systems in terms of their hydrodynamic characteristics. The torque delivered to the propellers and the thrust of the system were measured for different operation conditions of the propellers. These measurements lead to the hydrodynamic optimization of the ship propulsion system. The parameters under focus revealed the influence of distance between propeller planes, propellers' frequency of rotation ratio and type of propellers (co- or contra-rotating) for the overall efficiency of the system. Two of the ship propulsion systems under consideration were chosen, based on their hydrodynamic characteristics, for a detailed study of the swirling wake flow by means of laser Doppler anemometry.

A two-component laser Doppler system was employed for the velocity measurements. A light barrier mounted on the axle of the rear propeller motor supplied a TTL signal to mark the beginning of each period, thus providing angle information for the LDA measurements. Measurements were conducted for four axial positions in the slipstream of the pod drive models. The results show that wake of contra-rotating propeller is more homogeneous than when they co-rotate. In agreement with the results of the force/momentum measurements and with hypotheses put forward in the literature (see e.g., Breslin and Andersen (1996)), the co-rotating propellers model showed a much stronger swirl in the wake of the propulsor.

In addition the anisotropy of turbulence was analyzed using the anisotropy tensor introduced by Lumley and Newman (1977). The invariants of the anisotropy tensor of the wake flow were computed and were plotted in the Lumley-Newman-diagram. These measurements revealed that the anisotropy tensor in the wake of ship propellers is located near to the borders of the invariant map, showing a large degree of anisotropy. They will be presented and will be discussed with respect to applications of turbulence models to predict swirling wake flows.

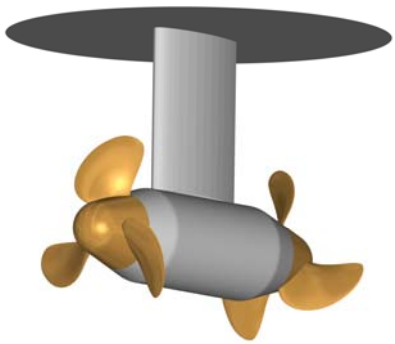

Figure 1: Contra-rotating propellers pod drive model

1 Introduction

Advancements in ship propulsion systems to increase their efficiency have reached a state of research and development that requires the combined employment of analytical, numerical and experimental techniques to reach many of the high pre-set aims put forward these days. These aims are usually set by the economy defined for the very large modern tankers and bulk carriers employed for ship transportations and this requires attention to be paid to the enhancement of the efficiency of ship propulsion systems. The obvious way to obtain an efficiency increase is the employment of propellers of large diameters driven by engines at low revolutions but such solutions are in many cases not practical. It is the optimization of the interaction of all these components that is the final aim of the propulsor design process. To answer to the demands of today's challenges it was felt that an experimental test facility is needed that permits model investigations to be carried out providing information on the torque and momentum for model ship propulsion systems and also on their efficiency. In addition, laser-Doppler measurements were felt to be needed in order to provide information on how the flow field is changing when a particular design of a propulsor is realized that shows a higher efficiency. It is for these reasons that an extended test facility was set up inside and around the water tunnel of LSTM-Erlangen consisting of torque and momentum measuring techniques as well as a complete laser-Doppler system. The facility is briefly described in Section 2 of this paper, focus being given to the LDA set-up.

Based on a design by Siemens AG, a set of 24 pod drive models were studied at the newly built ship propulsion research facility at LSTM (Pêgo *et al.* 2005). This research aimed to improve the efficiency of the propulsor, for which the produced thrust and delivered torque were measured in the water tunnel balance. Pod drive models with tandem inline co- and contra-rotating propellers were used for the experiments. The measurements have shown the influence of the pod geometry on the propulsor overall efficiency and also proved that contra-rotating propellers provide higher efficiency than co-rotating propellers. This increase of efficiency can be either used to increase the speed of the ship without increasing fuel consumption or to reduce the consumption of fuel without reducing the ship's speed.

Two of the models were chosen for a detailed study of the wake flow, those being the most efficient co- and contra-rotating propellers pod drive models, respectively. A two component LDA system was used to measure the mean flow and the turbulent flow quantities in the wake of these two models. Phase resolved laser Doppler anemometry measurements were conducted at different planes in the wake, showing the axial development of the flow in form of radial distributions of the mean flow components and the Reynolds stresses tensor components. Based on this data the invariants of the anisotropy of turbulence tensor were computed and plotted in the Lumley-Newman invariant map (Lumley and Newman 1977, Lumley 1978). Section 3 of the present paper describes the experimental setup used during the research. In section 4 the results achieved are presented and discussed. It will be shown that the state of turbulence in the wake flow of ship propellers is strongly anisotropic.

The presentation closes with recommendations for further research, especially in the field of numerical predictions of propeller flows. Present commercial codes are largely based in robust but simple turbulence models which make use of Boussinesq's eddy-viscosity assumption. They cannot take into account the anisotropy of turbulence in the flow and are thus inappropriate for swirling flows. It is suggested to adopt more complex models in the prediction of ship propeller flows, capable of correctly predicting the anisotropy of turbulence in the flow.

2 Test rig and measurement technique

2.1 Water tunnel

The experiments were performed in the water tunnel at LSTM-Erlangen, which is shown in figure 2. This facility is a closed loop water tunnel, whose most relevant elements are: water reservoir, axial pump, settling chamber and contraction cone, horizontal test section and return. In order to reduce the level of turbulence in the flow and homogenize the velocity distribution, a set of honeycombs and screens are placed in the settling chamber.

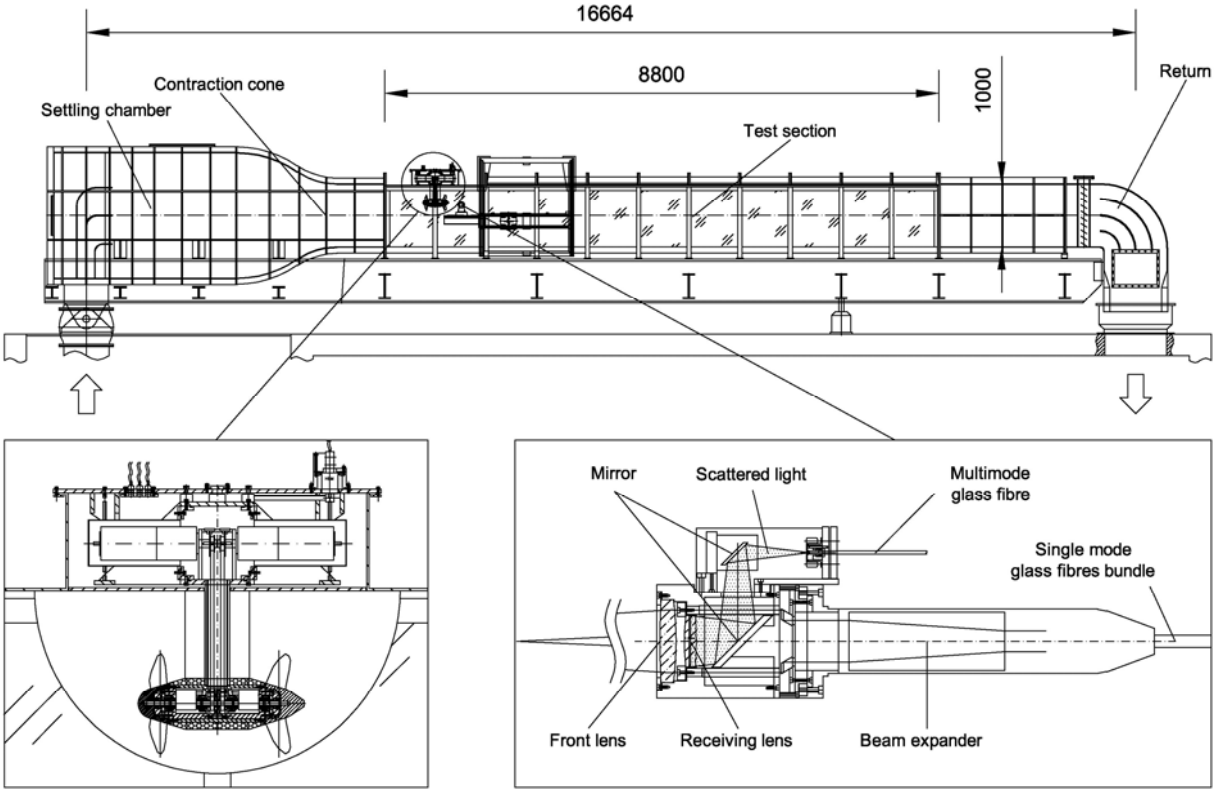

Figure 2: Water tunnel with ship propulsion test facility

The test section has a rectangular shape with a width of 800 mm and a height of 1000 mm in an extension of 8800 mm. Large windows of glass build the test section, thus providing unrestricted optical access to the interior. Continuous control of the flow rate in the test section is achieved by setting the pitch angle of the pump's impeller blades. The contraction cone, designed with the method suggested by Börger (1973, 1975), has a contraction ratio of 4 and a length of 1600 mm.

2.2 Ship propulsion models

The ship propulsion models tested were two types of pod drive models with co- and contra-rotating propellers, respectively. Figure 3 presents the most relevant components of the models, showing also the balance used for the force/momentum measurements to determine the pod drive models efficiency.

The inner housing of the ship propulsion system models accommodated in the upper stage two DC motors, which powered the ship propellers. There was a motor for each propeller, which allowed rotating the propellers independently from each other. This was, obviously, necessary for the experiments with contra-rotating propellers. For co-rotating propellers only one of the motors

was used, driving both propellers in synchronization. A toothed belt transmitted the power from motor shaft to propeller shaft without slip. The propeller's frequencies of revolution were coincident with the respective motor's frequency. A light barrier delivered a TTL signal marking the beginning of every new turn of the motor. This signal was used to measure the propeller's frequency and also for the phase-resolved LDA measurements.

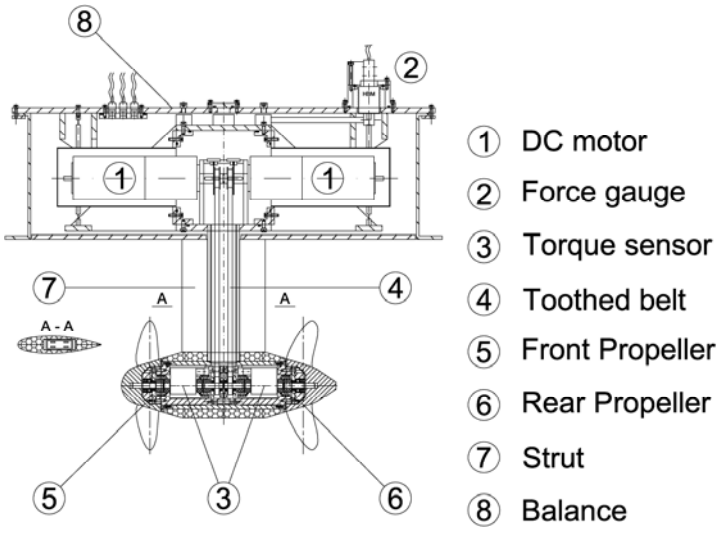

Figure 3: Pod drive model and water tunnel balance

The strut from which the pod is suspended has a vertical orientation and constant cross section, shaped in the form of an airfoil. The body of the pod is composed of a central section of cylindrical shape, cones at each end with fairing sections in between. The conical sections were designed as prolongation of the hub of the propellers in order to have a smooth flow transition between hub and pod.

As pod drives with co- and contra-rotating propellers were studied, there were two different pairs of propellers. A solution with three propellers was used. This was possible by using a common front propeller for both arrangements (co- and contra-rotating) and to have two different rear propellers, one with the same rotational sense as the front propeller and the other one with the opposite sense. The propellers had a diameter of 250 mm and were designed with the same criteria, apart from the rear propeller rotation sense. For the given propellers diameter the blockage ratio was 6% of the water tunnel test section.

2.3 LDA system and signal processing

For this set of measurements a two-component Aerometrics Phase Doppler Particle Analyser (PDPA) was adapted to operate as LDA. The base included a Spectra-Physics Stabilite 2017 Ion Laser operating in multiline mode, and a Fibre Drive from Aerometrics. A Bragg cell inside the Fiber drive spitted the laser beam in the 0 and -1 orders, which were then separated by two prisms into the different wavelengths, thus providing two blue (488.0 nm) and two green (514.5 nm) laser beams. The laser beams were transmitted by monomode polarization preserving glass fibers to the LDA probe. The original transmitting/receiving lens was substituted by a dedicated backscatter receiving optics, as shown in the right enclosure of figure 2. The probe created a measuring volume of about 100 μm diameter at a distance of 665 mm from the front lens in water. This set-up allowed simultaneous two-component velocity measurements in backscatter mode.

Light collected by the transmitting/receiving lens was focused by an achromatic lens onto the

end of a multimode fiber optics. The collected light was separated into the individual wavelengths by a Dantec color separator and then transmitted to two Dantec photomultipliers. The LDA signals were then processed by two Dantec 57N20 BSA enhanced units, operating in synchronous mode. The complete experimental set-up used during the LDA measurements is presented in the diagram of figure 4.

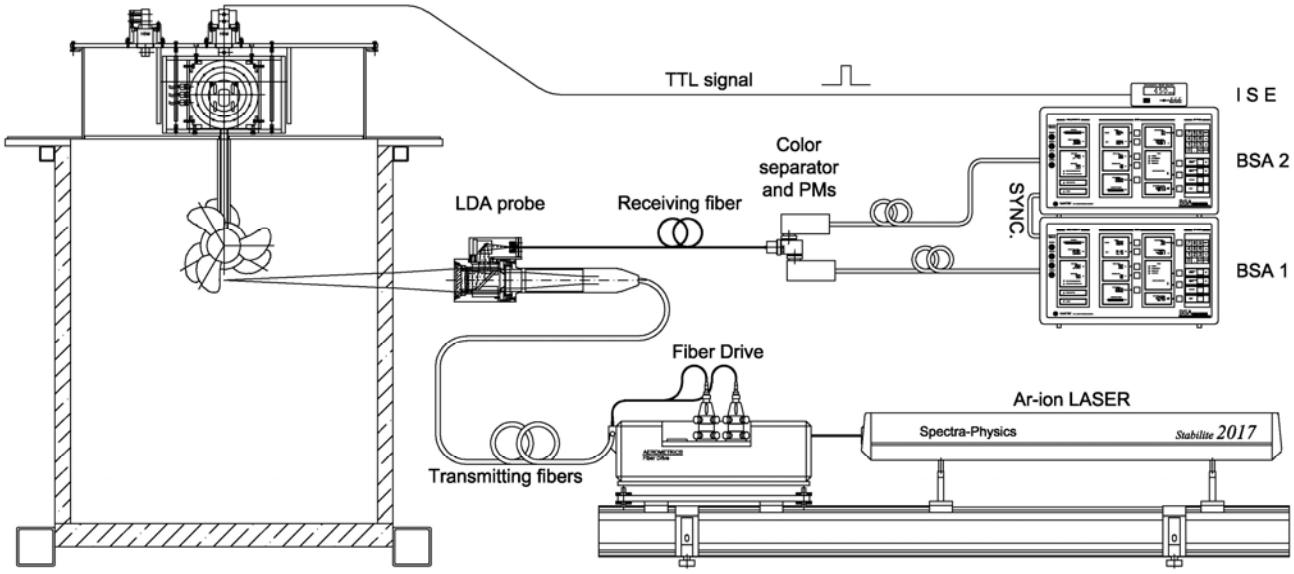

Figure 4: Experimental setup showing pod drive model in the water tunnel and the LDA system

3 Measurements

3.1 Coordinate Systems

In the tunnel-fixed frame of reference, the following coordinate systems were defined (the prime symbol was here used when referring to coordinates in the tunnel-fixed frame of reference):

- Cartesian coordinates *0x'y'z'*, where the *x'*-axis is along the propeller shaft centerline, pointing downstream, the *y'*-axis is set horizontal pointing starboard and the *z'*-axis is pointing upwards. The *y'z'*-plane coincides with the propeller plane.
- Cylindrical coordinates *0x'r'θ'*, where *r'* is radial outward and *θ'* goes counter-clockwise starting on the *y'*-axis when looking upstream. The coordinates in both systems are related by,

$$x' = x',$$
$$y' = r'\cos\theta',$$
$$z' = r'\sin\theta'.$$

In the propeller blade-fixed frame of reference the coordinates were:

- Cartesian coordinates *0xyz*, being the *y*-axis attached to one of the propeller blades.
- Cylindrical coordinates *0xrθ*.

The systems are related to each other by the following relationships:

$$x = x',$$
$$r = r',$$
$$\theta = \theta' - \omega t,$$
$$y = r\cos\theta = y'\cos\omega t + z'\sin\omega t,$$
$$z = r\sin\theta = z'\cos\omega t - y'\sin\omega t,$$

where ω is the angular speed of the propeller rotation, which was constant during the measurements. The coordinate systems are represented in figure 5 for easiness of interpretation.

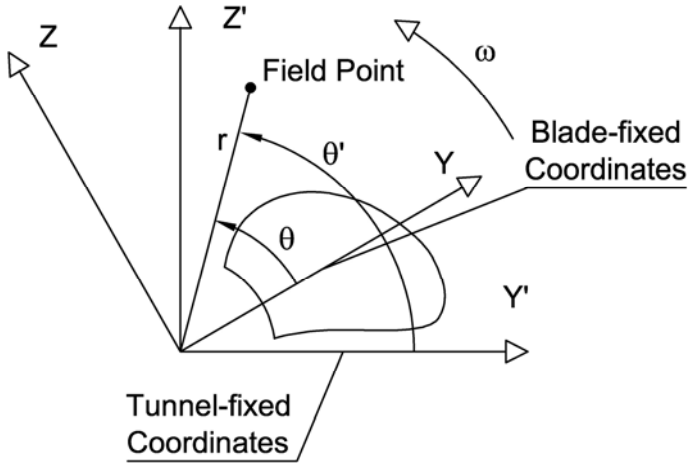

Figure 5: Coordinate systems (looking upstream)

3.2 Velocity Field Mapping

For the results described in the present paper the propellers frequency of revolution was set to 7.5 Hz in the co- as well as in the contra-rotating configuration. For the co-rotating propellers pod drive model the shafts of both the rear and the front propeller were driven by one single motor, so that the relative position between propellers was always constant during the experiment. In both cases the operation point of highest efficiency was considered.

Using the two-component LDA system it was possible to measure directly two simultaneous velocity components. The axial velocity, U_a, could be measured directly using one of the laser beam pairs. Using the axisymmetry of the flow the cylindrical velocity components were measured in the Cartesian coordinate system. Along the y-axis the vertical component of the velocity, U_Z, coincides with the tangential velocity, U_θ, thus, measuring radial profiles along this axis will result in tangential velocity distribution. In a similar manner U_Z coincides with the radial velocity, U_r, along the z-axis. The velocity distribution in the propeller wake is given by taking records of instantaneous velocities at a measurement position fixed with the tunnel. Since the propeller rotates, the position of the measuring volume relative to the propellers moves, thus giving the velocity distribution over the circumference.

Measurements were, typically, taken at 60 different radii. For radii, r, smaller than the propeller radius, R, the spacing between measuring points was 5 mm and for larger ones this was increased to 10 mm. For each measuring position a total number of 130.000 samples were collected. The data was then processed and statistically reduced by averaging the LDA measurements within

increments of 2° of propeller shaft angle. After hardware validation and statistical processing an average of about 1500 samples per radius and per angular position was obtained.

Measurements were taken at four axial positions, x/D =1, 2, 5 and 10, but only the results for the first and the third positions will be presented in this paper.

3.3 Anisotropy Invariant Map

It is well known that in many relevant flows the state of turbulence diverges from the isotropic state. For these flows the turbulent fluctuations present different characteristics according to the direction considered. In order to quantify the degree of anisotropy of the turbulent flow field Lumley and Newman (1977) introduced a new tensor, a_{ij}, defined as:

$$a_{ij} = \frac{\overline{u_i' u_j'}}{q^2} - \frac{1}{3}\delta_{ij},$$

where $\overline{u_i' u_j'}$ is the Reynolds stress tensor and $q^2 = \overline{u_i' u_i'}$, its trace. The second and third invariants of this tensor are given by,

$$II_a = a_{ij} a_{ji},$$
$$III_a = a_{ij} a_{jk} a_{ki},$$

and can be used to classify the state of turbulence in the flow by its degree of anisotropy. The anisotropy of turbulence tensor, a_{ij}, extracts from the Reynolds stress tensor the isotropic proprieties leaving just the anisotropic part of the tensor for analysis. For isotropic turbulence, $a_{ij} = 0$ and so $II_a = III_a = 0$. Analyzing the limiting states of turbulence, Lumley and Newman (1977) have built the map that is shown in figure 7 and postulated that all states of turbulence must be contained inside the borders of the triangle when expressed in the invariant space. The upper limit of the map, represented by the straight line,

$$II_a = \frac{2}{9} + 2III_a,$$

corresponds to the state of two-component turbulence and is typical for near-wall flows, where the normal flow component vanishes faster than the other two with the proximity of the wall. The left and the right branch of the map represent the axisymmetric state of turbulence, for which two components of the $\overline{u_i' u_j'}$ tensor are similar and the third is very different. When plotted in the map it is represented by the following equation,

$$II_a = \frac{3}{2}\left(\frac{4}{3}\left|III_a\right|\right)^{2/3}.$$

The left branch represents the axisymmetric contraction where two of the components are much bigger than the third. Finally, the right branch is representative of the axisymmetric expansion, where one of the Reynolds stresses is much bigger than the other two. Besides the isotropic state of turbulence, two other singular states exist, namely the isotropic two-dimensional turbulence and the one-dimensional turbulence. The highest degree of anisotropy that can be reached is for the latter

state, which corresponds to the point of the map furthest from the origin.

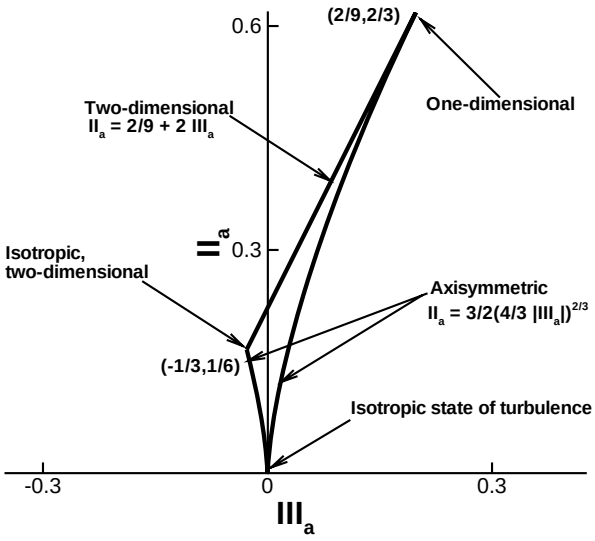

Figure 6: Lumley-Newman Invariant Map (Lumley and Newman (1977))

4 Discussion

4.1 Mean Flow

Figures 8 to 11 show the radial distribution of the mean axial and mean tangential velocity in the wake of the co- and contra-rotating propellers pod drive models respectively. For each component, the velocity distribution at two axial positions (x/D = 1 and x/D = 5) is provided. Each line represents an angular position in the blade-fixed frame of reference. To avoid a too dense graphic, only 6 of the 60 measured radial positions were plotted. Their location in the blade-fixed frame of reference is shown in figure 7 where the colors identify the lines of figures 8 to 11. All velocity components were normalized by the inflow velocity, V_a.

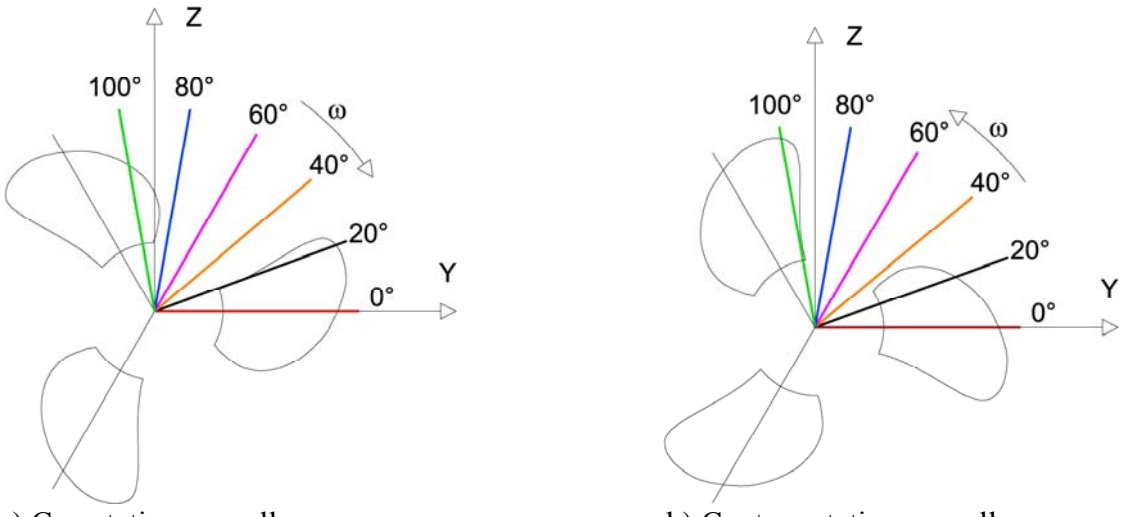

a) Co-rotating propellers b) Contra-rotating propellers

Figure 7: Position of radial profiles in the blade-fixed frame of reference

The idea of using contra-rotating propellers to improve the efficiency of the ship propulsor is triggered by the fact that the rear propeller can be used to regain some of the energy lost to the swirl in the slipstream of the front propeller. Contra-rotating propellers thus should produce higher thrust and weaker swirl. Comparing the results of the mean axial velocity at one diameter distance from the propeller it is clear how in the contra-rotating propellers pod drive model the axial momentum reaches higher values with more uniform distribution. The depression appearing closer to the axis of the propeller evidences the wake defect due to the hub and is deeper in the co-rotating propellers model. In both cases the tip vortex is made visible by a solid body rotation pattern in line $\theta = 80º$. This effect is also present in the mean tangential velocity component. As predicted by the theory, the tangential component of the co-rotating propellers pair is much stronger than that of the contra-rotating propellers model. In fact, while in the former case the distribution resembles the one of a concentrated swirl with a peak of half the value of the inflow velocity, the latter has a much smaller peak and less defined shape.

At five diameters distance from the propeller plane the angle dependency of the flow is much attenuated, which is recognized by the overlapping of the six curves into one. This results in a weak correlation between the rear propeller angular position and the flow field in the far wake. In both the co- and the contra-rotating propellers models the effect of distance in the axial momentum profile is to make it more uniform distribution and to flatten the depression in the axis, the latter evolving faster than the former.

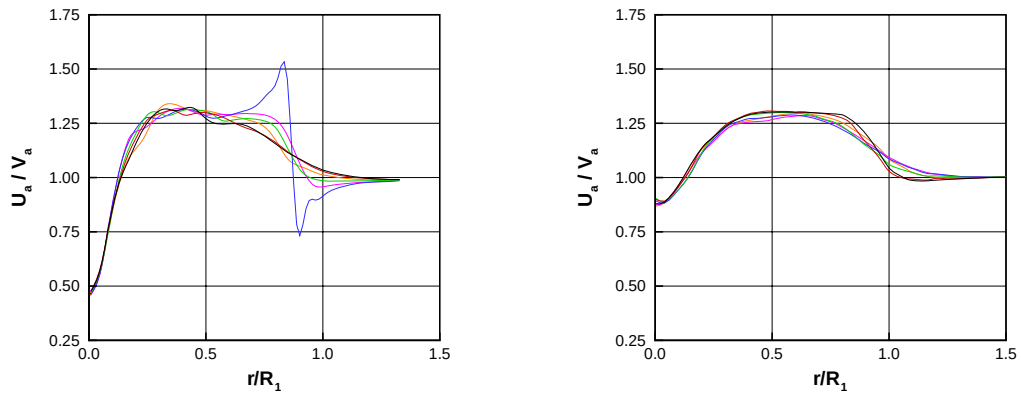

a) $x/D = 1$ $x/D = 5$

Figure 8: Axial velocity distribution in the wake of a co-rotating propellers pod drive model

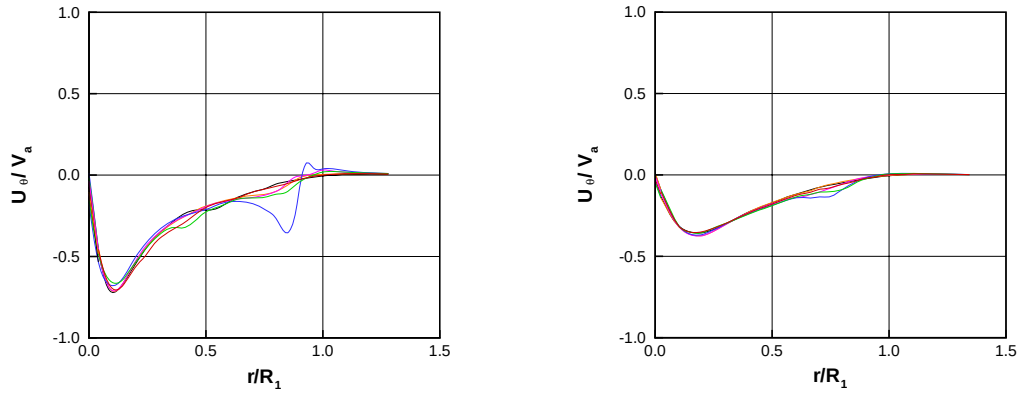

a) $x/D = 1$ $x/D = 5$

Figure 9: Tangential velocity distribution in the wake of a co-rotating propellers pod drive model

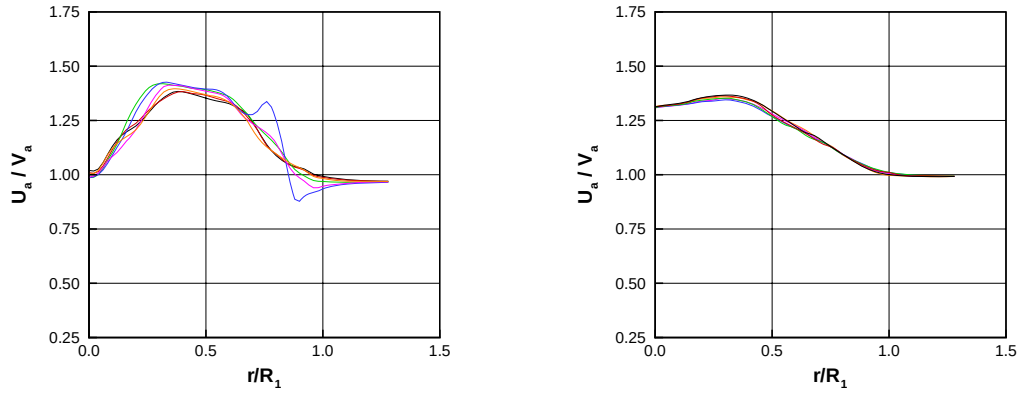

a) $x/D = 1$ $x/D = 5$

Figure 10: Axial velocity distribution in the wake of a contra-rotating propellers pod drive model

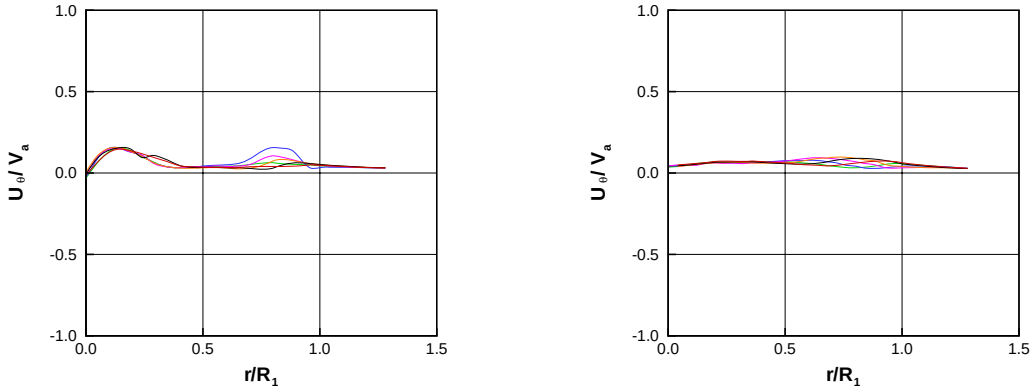

a) $x/D = 1$ $x/D = 5$

Figure 11: Tangential velocity distribution in the wake of a contra-rotating propellers pod drive model

4.2 Anisotropy of Turbulence

For the measurements introduced in the previous section the anisotropy tensor and its invariants were computed according to the definitions of section 3.3. The invariants were plotted in the invariant map and are presented in figures 12 and 13. In both the co- and the contra-rotating propellers the flow in the wake shows a tendency for anisotropic states of turbulence. At the position closest to the rear propeller (x/D = 1) the data covers the interior of the map and is relatively far apart from the borders. With the distance from the propeller the data converges and shows alignment with the right branch of the map, thus presenting characteristics of axisymmetric turbulence. The degree of turbulence is in both cases high, which can be derived by the high values of II_a and the existence of data close to the one-component turbulence state. The present measurements are in agreement with the literature on swirling flows in pipes (Steenbergen (1995), Pashtrapanska (2004)), which show the same trend in the invariant map. The results here presented alert for the fact that anisotropy of turbulence plays an important role in swirling flows and in particular in ship propeller flows. It is concluded, that for the numerical prediction of these flows the state of turbulence must be considered in the formulation of the employed turbulence model. The work of other authors supports this fact and shows that swirling flows still remain a not yet fully resolved field of research in the fluid mechanics (see for example Jakirlić et al. (1998), Jakirlić et al. (2002)).

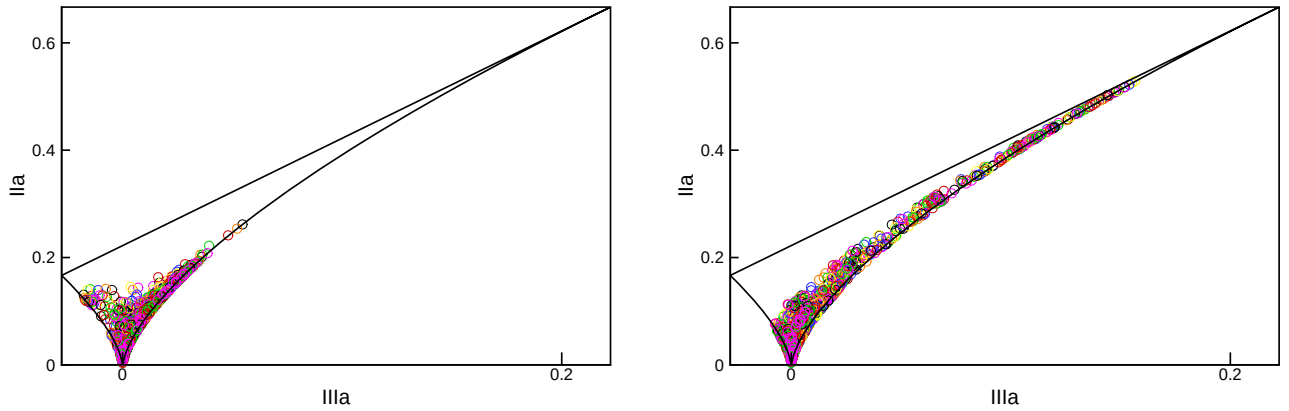

a) $x/D = 1$ $x/D = 5$

Figure 12: States of turbulence in the wake of the co-rotating propellers pod drive model (color identification is the same as in figure 7)

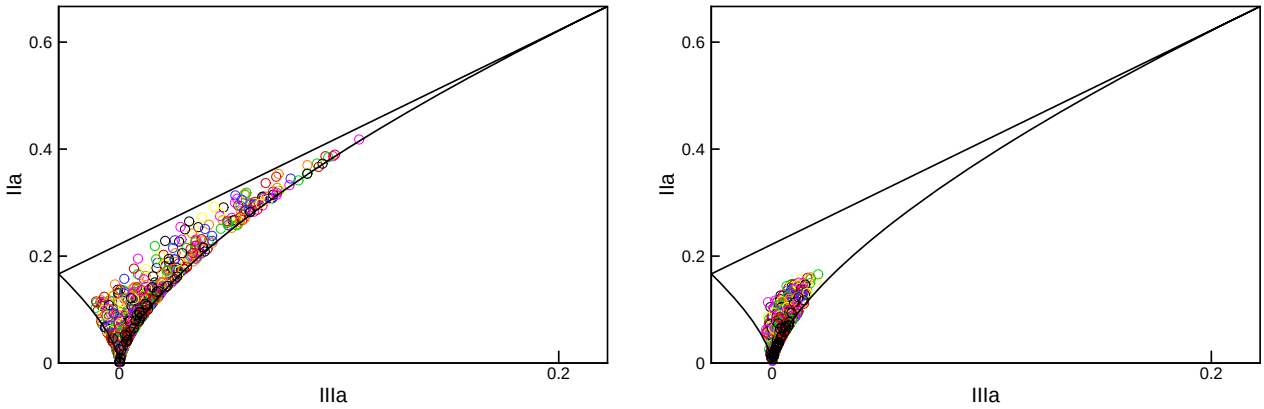

a) $x/D = 1$ $x/D = 5$

Figure 13: States of turbulence in the wake of the contra-rotating propellers pod drive model (color identification is the same as in figure 7)

5 Conclusions and remarks

A new experimental facility for the detailed research of ship propulsion systems has been introduced. The results of flow measurements using LDA in the slipstream of two pod drive models (with tandem co- and contra-rotating propellers, respectively) were presented for two measuring positions in the near and the far wake. The mean velocity field and anisotropy of turbulence were discussed.

It was shown that the characteristics of the flow are very different for the two configurations. It was proven that contra-rotation results in a much smaller swirl and higher momentum increase than co-rotating propellers. The influence of the propeller position in the slipstream flow vanishes with the distance to the propeller plane.

The analysis of the anisotropy of turbulence in the slipstream of the pod drive models reveals that the flow is strongly anisotropic. It is, thus, recommended to take this fact into consideration when predicting swirling flows by numerical methods.

Acknowledgements

The authors gratefully acknowledge the support of SIEMENS AG. to carry out the development work described in this paper. Support was also received through the Fundação para a Ciência e Tecnologia, Portugal, to finance the time of João Pedro Pêgo at LSTM-Erlangen, for which the authors express their gratefulness.

References

Börger, G.-G. (1975) Optimierung von Windkanaldüsen für den Unterschallbereich, Zeitschrift für Flugwissenschaften, 23 (2), 45-50

Breslin, J., Andersen, P. (1996) *Hydrodynamics of ship propellers*, Cambridge, Cambridge University Press

Jakirlić, S., Hanjalić, K., Tropea, C. and Volkert, J. (1998), *On the computation of rotating and swirling confined flows with second-moment closure models* AIAA Journal, 7th Symp. on Flow Modelling and Turbulence Measurements, Tainan, Taiwan, 315-324

Jakirlić, S., Hanjalić, K. and Tropea, C. (2002) *Modelling rotating and swirling turbulent flows: a perpetual challenge*, AIAA Journal, 40, 1984-1996

Lumley, J.L. (1970) *Toward a turbulent constitutive relation*, Journal of Fluid Mechanics, 41, 413-434

Lumley, J. L. and Newman, G. R. (1977) *The return to isotropy of homogeneous turbulence,* Journal of Fluid Mechanics, vol. 82, pp 161-178

Pashtrapanska, M. (2004) *Experimentelle Untersuchung der turbulenten Rohrströmungen mit abklingender Drallkomponente*, PhD thesis, Friedrich-Alexander University Erlangen-Nürnberg

Pêgo, J., Lienhart, H., Durst, F. and Badran, O. (2005) *Construction of a test facility for the research of ship propulsion systems*, Emirates Journal for Engineering Research, 10 (2), 1-8

Steenbergen, W. (1995) *Turbulent pipe flow with swirl*, PhD thesis, Eindhoven University of Technology.